



HJB-RBF Based Approach for the Control of PDEs

Alessandro Alla¹ · Hugo Oliveira² · Gabriele Santin³

Received: 26 April 2022 / Revised: 3 April 2023 / Accepted: 6 April 2023
© The Author(s), under exclusive licence to Springer Science+Business Media, LLC, part of Springer Nature 2023

Abstract

Semi-Lagrangian schemes for the discretization of the dynamic programming principle are based on a time discretization projected on a state-space grid. The use of a structured grid makes this approach not feasible for high-dimensional problems due to the curse of dimensionality. Here, we present a new approach for infinite horizon optimal control problems where the value function is computed using radial basis functions by the Shepard moving least squares approximation method on scattered grids. We propose a new method to generate a scattered mesh driven by the dynamics and the selection of the shape parameter in the RBF using an optimization routine. This mesh will help to localize the problem and approximate the dynamic programming principle in high dimension. Error estimates for the value function are also provided. Numerical tests for high dimensional problems will show the effectiveness of the proposed method.

Keywords Dynamic programming · Hamilton–Jacobi–Bellman equation · Optimal control for PDEs · Radial basis functions

Mathematics Subject Classification 49L20 · 93B52 · 65D12 · 65N06

1 Introduction

The classical Dynamic Programming (DP) approach to optimal control problems is based on the characterization of the value function as the unique viscosity solution of a Hamilton–Jacobi–Bellman (HJB) equation. The DP scheme for the numerical approximation of

✉ Alessandro Alla
alessandro.alla@unive.it

Hugo Oliveira
oliveira@mat.puc-rio.br

Gabriele Santin
gsantin@fbk.eu

¹ Dipartimento di Scienze Molecolari e Nanosistemi, Università Ca' Foscari Venezia, Venice, Italy

² Department of Mathematics, PUC-Rio, Rio de Janeiro, Brazil

³ Digital Society Center, Bruno Kessler Foundation, Trento, Italy

viscosity solutions of Bellman equations is typically based on a time discretization which is projected on a fixed state-space grid. The time discretization can be performed by a one-step scheme for the dynamics, and the projection on the grid typically uses a local interpolation. Clearly, the use of a grid is a limitation with respect to possible applications in high-dimensional problems due to the curse of dimensionality. We refer e.g. to [6, 22] for theoretical results and numerical methods.

We will consider in this paper a method based on positive definite kernels and in particular Radial Basis Functions (RBFs), which are a large class of methods that are extensively used in numerical analysis and scientific computing, including the solution of PDEs. We mainly mention here relevant applications to control problems. In [28], the HJB equation has been approximated by means of Shepard moving least square approximation, providing error estimates and convergence results. Numerical tests for a selected kernel and structured meshes have been provided for the control of low dimensional problems. A Kriging's interpolation was introduced in [14] with Halton meshes up to dimension 6. We also mention the use of RBFs in [12] for surface reconstruction. For a more detailed account of recent theoretical and application advances we refer the interested reader to [23, 24, 37], and to [13, 26] for an introduction to active research topics on RBF approaches for the solution of PDEs.

Our work is based in particular on [28], with the aim of extending the method to high dimensional problems, e.g. control of PDEs where the discretized dimension is at least of order 10^3 . We have investigated this approach on scattered meshes since the use of structured meshes is impossible for such high dimensional problems, and thus we resort to a grid driven by the dynamics of the problem, similarly to what is done in [3], where a tree structure has been proposed to approximate the finite horizon optimal control problem and the time dependent HJB equation. The generation of the grid driven by the dynamics will help us to compute an approximate value function for some region of interests, and then feedback controls for a class of initial conditions. This is an important novelty in the field, since many works in the literature for high dimensional problems are strictly linked to a single initial condition, see e.g. [3, 30].

Within the RBF approximant, the determination of the kernel's shape parameter is known to be a crucial problem. Several techniques exist in the literature to optimize this parameter (see e.g. Chapter 14 in [24] for a recent survey), but they are usually based on the minimization of the approximation error. We introduce instead a novel technique based on the residual of the HJB equation.

Specifically, even if the reconstruction of the function requires the computation of several Shepard approximant, a unique parameter is globally optimized based on the residual of the Value Iteration scheme. The use of the residual in HJB has been introduced in [29] and also used in the context of RBF and HJB to obtain an adaptive grid [25]. Here, the residual is used as quantity of interest to select the shape parameter.

We summarize the main contributions of our paper and the novelty of our approach:

1. Generation of an unstructured mesh driven by the dynamics that helps us to localize the problem.
2. An optimized way to select the shape parameter minimizing the residual of the Value Iteration method.
3. The possibility to compute feedback control of PDEs for a class of initial conditions.¹
4. An error estimate of the reconstruction process that is valid along trajectories of the dynamics.

¹ We remark that, although it is well-known how to compute feedback controls by semi-Lagrangian schemes, this is not trivial for high dimensional problems, as already mentioned earlier in the introduction.

Let us briefly comment on related literature on the control of PDEs using a DP approach. In the last two decades there has been a tremendous effort to mitigate the curse of dimensionality with the goal to control PDEs. It is straightforward to see that the discretization of a PDE leads to a large system of ODEs which is hard to control using a DP approach. The first method is related to the combination of Model Order Reduction techniques and dynamic programming. The idea is to use a projection technique, e.g. Proper Orthogonal Decomposition ([7]) to reduce the dimension of the dynamical systems. Then, we can approximate with a standard Value Iteration algorithm the corresponding reduced HJB equation. This turns out to be efficient if the reduction is up to dimension 4 or 5. We refer to the pioneer work [31] and to [4] for error estimates of the method. A different way to reduce the dimension of the dynamical system is given by pseudo-spectral methods as shown in [30]. Recently, the solution of HJB on a tree structure has been proposed in [3] and its coupling with Model Order Reduction in [5]. Other methods concern e.g. the use of sparse grids for time dependent Hamilton-Jacobi equations [8] and for the control of wave equations with a DP approach [27], tensor train decomposition [17, 18], neural networks [15, 16], and max-plus algebra [33, 34], and the direct approximation of the value function with kernel models trained on trajectories computed by solving many open-loop problems [19, 20, 35]. All these approaches are important contributions on the mitigation of the curse of dimensionality.

The outline of this paper is as follows. In Sect. 2 we recall the background of the DP approach. Section 3 concerns RBF interpolation and Shepard approximation. In Sect. 4, we propose the novel method for the coupling between RBF and DP. We will discuss and comment the details of our approach. Numerical simulations for the control of two different PDEs are shown in Sect. 5. Finally, conclusions and future works are driven in Sect. 6.

2 Dynamic Programming Equations

This section summarizes the main results for infinite horizon control problems by means of dynamic programming equations. For a complete description we refer e.g. to the manuscripts [6, 22].

In the paper, we will denote by Ω a compact subset of \mathbb{R}^d . Moreover, we will make the following assumptions, which are valid throughout the paper.

Assumption 1 The functions f and g are as follows.

- The function $f : \mathbb{R}^d \times \mathbb{R}^m$ from (2.1) is continuous with respect to the second argument and Lipschitz-continuous in the first argument, i.e. there exists a constant $L_f > 0$ such that

$$\|f(y, u) - f(\bar{y}, u)\|_2 \leq L_f \|y - \bar{y}\|_2 \quad \forall y, \bar{y} \in \mathbb{R}^d, u \in U.$$

- The function f is bounded by a constant M_f such that

$$\max \|f(y, u)\|_\infty \leq M_f, \quad \forall y \in \Omega \subset \mathbb{R}^d, u \in U.$$

- The running cost $g : \mathbb{R}^d \times \mathbb{R}^m \rightarrow \mathbb{R}^d$ is continuous in the second argument and Lipschitz continuous in the first argument, with Lipschitz constant $L_g > 0$.
- The function g is also bounded: $\|g(y, u)\|_\infty \leq M_g, \quad \forall y \in \Omega \subset \mathbb{R}^d, u \in U$.

Let the dynamical system be described by

$$\begin{cases} \dot{y}(t) = f(y(t), u(t)), & t \in (0, \infty], \\ y(0) = x \in \mathbb{R}^d, \end{cases} \quad (2.1)$$

where $y : (0, \infty] \rightarrow \mathbb{R}^d$ is the state variable, and the control is such that $u \in \mathcal{U}$ where $\mathcal{U} := \{u : (0, \infty] \rightarrow U, \text{ measurable}\}$ is the set of admissible controls, and $U \subset \mathbb{R}^m$ is a compact set. Under such hypothesis, together with Assumption 1, the existence of a unique solution to the system (2.1) holds true (see [22]).

We define the cost functional $\mathcal{J}_x : \mathbb{R}^d \times \mathcal{U} \rightarrow \mathbb{R}$ as

$$\mathcal{J}_x(y, u) := \int_0^\infty g(y_x(s), u(s))e^{-\lambda s} ds. \tag{2.2}$$

The constant $\lambda > 0$ is a discount factor, the term $e^{-\lambda s}$ guarantees the convergence of the integral for g bounded, and $y_x(s)$ denotes the solution of (2.1). We will use the subscript x in our notations to stress the dependence on the initial condition.

With these definitions, our optimal control problem reads:

$$\min_{u \in \mathcal{U}} \mathcal{J}_x(y, u), \tag{2.3}$$

with y being a trajectory that solves (2.1) with initial point x and control u . We aim at obtaining the control in a feedback form and, for this reason, we define the value function as

$$v(x) := \inf_{u \in \mathcal{U}} \mathcal{J}_x(y, u). \tag{2.4}$$

One can characterize this function in terms of the Dynamical Programming Principle (DPP), i.e.,

$$v(x) = \inf_{u \in \mathcal{U}} \left\{ \int_0^\tau g(y_x(s), u(s)) e^{-\lambda s} ds + e^{-\lambda \tau} v(y_x(\tau)) \right\} \quad \forall x \in \mathbb{R}^d, \tau > 0. \tag{2.5}$$

From (2.5), we derive the Hamilton–Jacobi–Bellman (HJB) equations corresponding to the infinite horizon problem, that is

$$\lambda v(x) + \sup_{u \in U} \{-f(x, u) \cdot \nabla v(x) - g(x, u)\} = 0, \quad x \in \mathbb{R}^d, \tag{2.6}$$

where ∇v is the gradient of v . The HJB is a further characterization of the value function by means of a non linear PDE whose solution has to be understood in the viscous sense [6]. Typically, v is a Lipschitz continuous function. Thus, if one is able to solve (2.6), it is possible to obtain the optimal feedback control $u^*(x)$:

$$u^*(x) = \arg \max_{u \in U} \{-f(x, u) \cdot \nabla v(x) - g(x, u)\}, \quad x \in \mathbb{R}^d. \tag{2.7}$$

3 Radial Basis Functions and the Shepard method

This section presents a brief explanation of Radial Basis Functions (RBFs) and the Shepard approximation method. Most of the following material is based on the book [23] for the general RBF theory, and on the paper [28] for the Shepard method, to which we refer for further details. A RBF $\varphi : \mathbb{R}_{\geq 0} \rightarrow \mathbb{R}$ can be used to define a radially invariant function $\mathbb{R}^d \ni x \mapsto \varphi(\|x\|_2)$, which is usually required to be positive definite, meaning that the associated matrix $K_X := (\varphi(\|x_i - x_j\|))_{i,j=1}^N \in \mathbb{R}^{N \times N}$ is positive semidefinite for any set $\{x_i\}_{i=1}^N$ of points. Several choices exist for a function φ with these properties (see e.g. [23]). In this paper we will consider only radially compactly supported RBFs. A significant example

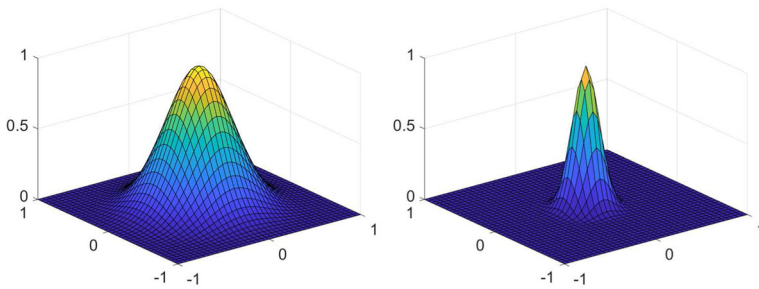


Fig. 1 Wendland function with $\sigma = 0.8$ (left) and $\sigma = 2$ (right)

are the Wendland RBFs, which are a family of strictly positive definite² RBFs of compact support and of different smoothness, depending on a parameter (see [36]). The radial nature of these bases can be used to tune their spread by means of a shape parameter $\sigma > 0$, i.e., usually one works with a basis $\varphi^\sigma(r) := \varphi(\sigma r)$, $r \in \mathbb{R}_{\geq 0}$. Figure 1 shows the radial function $\varphi^\sigma(\|x\|_2)$ resulting from the Wendland RBF

$$\varphi(r) := (\max\{0, 1 - r\})^6 (35r^2 + 18r + 3), \tag{3.1}$$

with $\sigma = 0.8$ on the left panel and $\sigma = 2$ on the right panel. We can see how the parameters influence the *shape* of the basis functions and makes it flat (left) or spiky (right). The RBF is scaled so that $\varphi^\sigma(0) = 1$.

RBFs can be used as a tool in interpolation and approximations methods in a mesh-free environment. For this we consider a continuous function $\tilde{f} : \Omega \rightarrow \mathbb{R}$ with $\Omega \subset \mathbb{R}^d$ and a set of pairwise distinct approximation points (or nodes) $X := \{x_1, \dots, x_n\} \subset \Omega$ and the corresponding function evaluations. In this paper we use RBFs in a moving-least squares mode within a Shepard approximation scheme (see e.g. Chapter 23 in [23]). In this case, the RBF bases are used to form n weights

$$\psi_i^\sigma(x) := \frac{\varphi^\sigma(\|x - x_i\|_2)}{\sum_{j=1}^n \varphi^\sigma(\|x - x_j\|_2)}, \quad 1 \leq i \leq n, \tag{3.2}$$

and the Shepard approximant $S^\sigma[\tilde{f}](x)$ is formed as

$$S^\sigma[\tilde{f}](x) := \sum_{i=1}^n \tilde{f}(x_i) \psi_i^\sigma(x). \tag{3.3}$$

We remark that $S^\sigma[\tilde{f}]$ is not exactly interpolating the data, unless σ is chosen such that the functions ψ_i^σ have pairwise disjoint support. Observe that each $\psi_i(x)$ is compactly supported in $B(x_i, 1/\sigma) \subset \Omega$ and non negative, and the weights form a partition of unity, i.e., $\sum_{i=1}^n \psi_i^\sigma(x) = 1$ for all $x \in \Omega_{X,\sigma}$ with

$$\Omega_{X,\sigma} := \bigcup_{x \in X} B(x, 1/\sigma) \subset \mathbb{R}^d. \tag{3.4}$$

This implies that $S^\sigma[\tilde{f}](x)$ is actually a convex combination of the function values. Moreover, the compact support of the weights leads to a computational advantage and a localization. In particular, the Shepard weights are evaluated by constructing a distance vector $D \in \mathbb{R}^n$

² Strictly positive definite functions are such that the associated matrix K_X is positive definite.

with $D_i := \|x - x_i\|_2$ by computing only the weights ψ_i^σ such that $\|x - x_i\| \leq 1/\sigma$. This operation can be implemented by a range search.

An additional advantage of the Shepard method is that the construction of the approximant (3.3) can be directly obtained from the function values and the evaluation of the weights, without solving any linear system.

As RBF-based methods work with unstructured meshes, to obtain error estimates in this context it is common to consider the *fill distance* and the *separation distance*

$$h := h_{X,\Omega} := \sup_{x \in \Omega} \min_{x_i \in X} \|x - x_i\|, \quad q := q_X := \min_{x_i \neq x_j \in X} \|x_i - x_j\|.$$

The fill distance replaces the mesh size and it is the radius of the largest ball in Ω which does not contain any point from X , and it gives a quantification of the well spread of the approximation nodes in the domain. On the other hand, the separation distance quantifies the minimal separation between different approximation points. We remark that for any sequence of points it holds $\frac{1}{2}q \leq h$, but the inverse inequality $h \leq cq$, $c > 0$, does not hold unless the points are asymptotically uniformly distributed.

General error statements for Shepard approximation can be found in [23]. In this paper we will work with the result of [28], that we will recall in the following.

4 The Coupling Between DP and RBF

To overcome the difficulty of solving analytically Eq. (2.6), in this section we introduce the core approach of our work. We first recall the semi-Lagrangian discretization of (2.6) by means of Shepard approximation, then we propose a method to generate unstructured meshes, we define a strategy to select the shape parameter, derive error estimates of the overall approximation method and, finally, we summarize everything in one algorithm.

We remark that for the purpose of numerical computation we consider only finite horizons $t \in [0, T]$ with a given $T > 0$ large enough to simulate the infinite horizon problem. We also assume that the dynamics evolve for each initial value and control parameter within a compact set $\Omega \subset \mathbb{R}^d$ (see Assumption 2 later).

Moreover, we would like to stress that the algorithmic ideas introduced in the following may be of interest also when applied to other local approximation methods, and are not necessarily bounded to the RBF-based Shepard method introduced in Sect. 3. In particular, the application of a semi-Lagrangian scheme, the construction of the scattered mesh, and the technique for parameter optimization that are discussed in the following sections can all be applied together with any approximation method that can work on high-dimensional and scattered meshes.

4.1 Semi-Lagrangian Scheme for (2.6)

We first choose a temporal step size $\Delta t > 0$ and build a grid in time such that $t_k = k \Delta t$ with $k \in \mathbb{N}$. We will discuss in the following how to define a spatial discretization, and for now we just denote it as $X = \{x_1, x_2, \dots, x_n\} \subset \Omega$. Furthermore, the set U is discretized by replacing $u \in U$ with a piecewise constant control, i.e., for all $t \in [t_k, t_{k+1})$ we set $u(t) = u_k$ for some $u_k \in \mathbb{R}^m$. To introduce the approximation of the value function, we represent the Shepard approximant as an operator

$$S^\sigma : (L^\infty, \|\cdot\|_\infty) \rightarrow (\mathcal{W}, \|\cdot\|_\infty), \quad (4.1)$$

where $\mathcal{W} = \text{span}\{\psi_1^\sigma, \psi_2^\sigma, \dots, \psi_n^\sigma\}$ as in (3.2). We remark that the Shepard method uses as approximation nodes the same points X defined above. Moreover, we will discuss later (Sect. 4.3) a proper choice of σ in this case. Observe that the Shepard method is known to have potentially some diffusive behavior (see [25]), which would reduce the accuracy of the approximation especially in the case of singular solutions. We will comment on this point when discussing the numerical experiments.

We aim at the reconstruction of the vector $\{V_j\}_{j=1}^n \in \mathbb{R}^n$ where V_j is the approximate value for $v(x_j)$ for each $x_j \in X$. The full discretization of Eq. (2.6) is obtained starting from a classical approach (see e.g. [22]), but replacing as in [28] the local linear interpolation operator on a structured grid with the Shepard approximation operator. This discretization reads

$$V_j = [W_\sigma(V)]_j := \min_{u \in U} \left\{ \Delta t g(x_j, u) + (1 - \Delta t \lambda) S^\sigma[V](x_j + \Delta t f(x_j, u)) \right\}. \tag{4.2}$$

To compute V_j the set U is discretized in a finite number $M \in \mathbb{N}$ of points $U := \{u_1, \dots, u_M\}$, and the minimum is computed by comparison.

The full approximation scheme of the function is known as the Value Iteration (VI) method, and it is obtained by iteration of (4.2), i.e.,

$$V^{k+1} = W_\sigma(V^k), \quad k = 0, 1, \dots \tag{4.3}$$

To ensure convergence of the scheme it is necessary that W_σ is a contraction. In this context, the Shepard operator offers another striking benefit in comparison with plain RBF interpolation. Indeed, S^σ in (4.1) has unit norm as an operator from $(L^\infty, \|\cdot\|_\infty)$ to $(\mathcal{W}, \|\cdot\|_\infty)$, and this implies that the right hand side of (4.2) is a contraction if $\Delta t \in (0, 1/\lambda]$ (see [28] for the details, and especially Lemma 2). Therefore, the convergence of the value iteration scheme is guaranteed. The stopping criteria for (4.3) is given by

$$\|V^{k+1} - V^k\| < tol_V \tag{4.4}$$

for a given threshold $tol_V > 0$.

As soon as we obtain an approximation of the value function, we can compute an approximation of the feedback control as

$$u_n^*(x) = \arg \min_{u \in U} \{ \Delta t g(x, u) + (1 - \lambda \Delta t) S^\sigma[V](x + \Delta t f(x, u)) \}, \tag{4.5}$$

with $x = y(t_n)$. Thus, we are able to perform an approximate reconstruction of an optimal trajectory y^* and optimal control u^* .

Under the assumption that the fill distance h decays to zero and that the shape parameter scales as $\sigma = \theta/h$, in [28] it is proven that this approximation scheme converges. More precisely, under suitable assumptions on f and g , Theorem 3 in [28] guarantees that $\|v - V\|_\infty \leq (C/\theta)h$, where $C > 0$ depends on the dynamics but not on the discretization.

Despite these convincing theoretical guarantees, the requirement that $h = h_{X, \Omega}$ decays to zero is too restrictive in our setting, since a filling of the entire Ω may be out of reach for high dimensional problems. Moreover, as already mentioned in Sect. 3, the Shepard method performs an approximation in high dimensions and unstructured grids, while in [28] the authors focused on a given configuration for the shape parameter and an equidistant grid. In the next paragraphs we will explain how to select the shape parameter and to generate unstructured meshes to solve high dimensional problems. We remark that this approach can be also used for minimum time problem as we will see in Sect. 5. We refer to e.g. [6] and [2] for more details on the minimum time problem and its discretization scheme.

Remark 1 To ease the presentation we have used a forward Euler method to approximate the dynamical system (2.1). However, one can use other approaches such as e.g. high order one step methods or implicit methods. We refer e.g. to [21] for more details. Later, in the numerical tests we will use a backward Euler scheme to approximate the PDEs studied to guarantee the numerical stability of the method.

4.2 On the Scattered Mesh

Different possibilities are available for the definition of the discretization X of the spatial domain. A standard choice is to use an equi-distributed grid, which covers the entire space and usually provides accurate results for approximation problems. Unfortunately, for higher dimensional problems it is impossible to think to work on equi-distributed grid, as their size grows exponentially. This is a particular limitation in our case, since our goal is to control PDEs, whose discretization leads to high dimensional problems e.g. $d > 10^3$. On the other hand, a random set of points is computationally efficient to generate and to use, but in this case additional care should be taken because the distribution of points can be irregular (some regions can be more densely populated than others) and the fill distance may decrease only very slowly when increasing the number of points.

In general terms, there is a tradeoff between keeping the grid at a reasonable size and the need to cover the relevant part of the computational domain. In particular, it is well known that the fill distance for any sequence of points $\{X_n\}_{n \in \mathbb{N}}$ can at most decrease as $h \leq c_\Omega n^{-1/d}$ in \mathbb{R}^d for a suitable constant $c_\Omega > 0$ depending only on the geometry of the domain. Observe that uniform points have precisely this asymptotic decay of the fill distance. Thus, an exponentially growing number of points is required to obtain a good covering of Ω as d increases.

The key point to overcome these limitations is to observe that the evolution of the system provides itself an indication of the regions of interest within the domain. Following this idea, we propose a discretization method driven by the dynamics of the control problem (2.1). Observe that a similar idea has been used in [35] to compute the value function along the trajectories of open loop control problems. Moreover, in [3] the grid has been generated by points of the dynamics leading to the solution of the HJB equation on a tree structure. We stress once again that this kind of approach is an effective way to address the curse of dimensions, since only the parts of the space that are visited by some system trajectories are considered, without the need of filling the entire space. This of course is possible at the price of having a local approximation, but this locality is taken in full account in the following estimates, so that one can find a balance between the efficiency of the method and the coverage of the domain.

To define our dynamics-dependent grid we fix a time step $\overline{\Delta t} > 0$, a maximum number $\overline{K} \in \mathbb{N}$ of discrete times and, for $\overline{L}, \overline{M} > 0$, some initial conditions of interest and a discretization of the control space, i.e.,

$$\overline{X} := \{\bar{x}_1, \bar{x}_2, \dots, \bar{x}_{\overline{L}}\} \subset \Omega, \quad \overline{U} := \{\bar{u}_1, \bar{u}_2, \dots, \bar{u}_{\overline{M}}\} \subset U.$$

Observe that all these parameters do not need to coincide with the ones used in the solution of the value iteration (4.2), but are rather only used to construct the grid. Moreover, in general we use $\overline{\Delta t} > \Delta t$ and $\overline{M} < M$, i.e., the discretization used to construct the mesh is coarser than the one use to solve the control problem.

For a given pair of initial condition $\bar{x}_i \in \bar{X}$ and control $\bar{u}_j \in \bar{U}$, we solve numerically for $i = 1, \dots, \bar{L}$ and $j = 1, \dots, \bar{M}$ Eq. (2.1) to obtain trajectories

$$\begin{aligned} x_{i,j}^{k+1} &= x_{i,j}^k + \bar{\Delta}t f(x_{i,j}^k, \bar{u}_j), \quad k = 1, \dots, \bar{K} - 1, \\ x_{i,j}^1 &= \bar{x}_i, \end{aligned} \tag{4.6}$$

such that $x_{i,j}^k$ is an approximation of (2.1) with initial condition \bar{x}_i , constant control $u(t) = \bar{u}_j$, at time $t = k\bar{\Delta}t$. For each pair (\bar{x}_i, \bar{u}_j) we obtain the set $X_{\text{traj}}(\bar{x}_i, \bar{u}_j) := \{x_{i,j}^1, \dots, x_{i,j}^{\bar{K}}\}$ containing the discrete trajectory, and our mesh is defined as

$$X := X(\bar{X}, \bar{U}, \bar{\Delta}t, \bar{K}) := \bigcup_{i=1}^{\bar{L}} \bigcup_{j=1}^{\bar{M}} X_{\text{traj}}(\bar{x}_i, \bar{u}_j). \tag{4.7}$$

This choice of the grid is particularly well suited for the problem under consideration, as it does not aim at filling the space Ω , but instead it provides points along trajectories of interest. In this view, the values of $\bar{X}, \bar{U}, \bar{\Delta}t, \bar{K}$ should be chosen so that X contains points that are suitably close to the points of interest for the solution of the control problem. In the following proposition we provide a quantitative version of this idea, that will be the base of our error estimate in Theorem 2.

Proposition 1 *Let $X := X(\bar{X}, \bar{U}, \bar{\Delta}t, \bar{K})$ be the dynamics-dependent mesh of (4.7), and assume that f is uniformly bounded i.e., there exist $M_f > 0$ such that*

$$\sup_{x \in \Omega, u \in U} \|f(x, u)\| \leq M_f.$$

Then for each $x \in X, \Delta t > 0$ and $u \in U$ it holds

$$\text{dist}(x + \Delta t f(x, u), X) \leq M_f \Delta t. \tag{4.8}$$

Assume furthermore that f is uniformly Lipschitz continuous in both variables, i.e., there exist $L_x, L_u > 0$ such that

$$\begin{aligned} \|f(x, u) - f(x', u)\| &\leq L_x \|x - x'\| \quad \forall x, x' \in \Omega, \quad u \in U, \\ \|f(x, u) - f(x, u')\| &\leq L_u \|u - u'\| \quad \forall x \in \Omega, \quad u, u' \in U. \end{aligned}$$

Then, if $x := x^k(x_0, u, \Delta t) \in \Omega$ is a point on a discrete trajectory with initial point $x_0 \in \Omega$, control $u \in U$, timestep $\Delta t > 0$, and time instant $k \in \mathbb{N}, k \leq \bar{K}$, it holds

$$\text{dist}(x, X) \leq \left(|\Delta t - \bar{\Delta}t| \bar{K} M_f + \min_{\bar{x} \in \bar{X}} \|\bar{x} - x_0\| + \bar{K} \bar{\Delta}t L_u \min_{\bar{u} \in \bar{U}} \|\bar{u} - u\| \right) e^{\bar{K} \bar{\Delta}t L_x}. \tag{4.9}$$

Proof If $x \in X$ we simply have

$$\begin{aligned} \text{dist}(x + \Delta t f(x, u), X) &= \min_{x' \in X} \|x + \Delta t f(x, u) - x'\| \leq \|x + \Delta t f(x, u) - x\| \\ &= \Delta t \|f(x, u)\| \leq M_f \Delta t, \end{aligned}$$

which gives the bound (4.8) using only the boundedness of f .

To prove (4.9) we need to work explicitly with the initial points and the control values. By assumption we have

$$x = x^k(x_0, u, \Delta t) = x_0 + \Delta t \sum_{p=0}^{k-1} f(x^p(x_0, u, \Delta t), u).$$

Moreover, using (4.7) let $x' \in X$ be defined as

$$x' = x_{\ell,m}^k = \bar{x}_\ell + \overline{\Delta t} \sum_{p=0}^{k-1} f(x_{\ell,m}^p, \bar{u}_m),$$

for some $\ell \in \{1, \dots, \bar{L}\}$, $m \in \{1, \dots, \bar{M}\}$, and with $x_{\ell,m}^0 = x_0$.

It follows that

$$\begin{aligned} x^k(x_0, u, \Delta t) - \bar{x}_{\ell,m}^k &= x_0 - \bar{x}_\ell \\ &\quad + \Delta t \sum_{p=0}^{k-1} f(x^p(x_0, u, \Delta t), u) - \overline{\Delta t} \sum_{p=0}^{k-1} f(x_{\ell,m}^p, \bar{u}_m), \end{aligned}$$

and thus adding and subtracting $\overline{\Delta t} \sum_{p=0}^{k-1} f(x^p(x_0, u, \Delta t), u)$ gives

$$\begin{aligned} \|x^k(x_0, u, \Delta t) - x_{\ell,m}^k\| &\leq \|x_0 - \bar{x}_\ell\| + |\Delta t - \overline{\Delta t}| \sum_{p=0}^{k-1} \|f(x^p(x_0, u, \Delta t), u)\| \\ &\quad + \overline{\Delta t} \sum_{p=0}^{k-1} \|f(x^p(x_0, u, \Delta t), u) - f(x_{\ell,m}^p, \bar{u}_m)\| \\ &\leq \|x_0 - \bar{x}_\ell\| + |\Delta t - \overline{\Delta t}| k M_f \\ &\quad + \overline{\Delta t} \sum_{p=0}^{k-1} \|f(x^p(x_0, u, \Delta t), u) - f(x_{\ell,m}^p, \bar{u}_m)\|. \end{aligned}$$

Now adding and subtracting $f(x^p(x_0, u, \Delta t), \bar{u}_m)$ in the sum, and using the Lipschitz continuity of f , we get

$$\begin{aligned} \|x^k(x_0, u, \Delta t) - x_{\ell,m}^k\| &\leq \|x_0 - \bar{x}_\ell\| + |\Delta t - \overline{\Delta t}| k M_f \\ &\quad + \overline{\Delta t} \sum_{p=0}^{k-1} (L_u \|u - \bar{u}_m\| + L_x \|x^p(x_0, u, \Delta t) - x_{\ell,m}^p\|) \\ &= \|x_0 - \bar{x}_\ell\| + |\Delta t - \overline{\Delta t}| k M_f + k \overline{\Delta t} L_u \|u - \bar{u}_m\| \\ &\quad + \overline{\Delta t} L_x \sum_{p=0}^{k-1} \|x^p(x_0, u, \Delta t) - x_{\ell,m}^p\|. \end{aligned}$$

Applying the discrete Grönwall lemma to this inequality gives

$$\|x^k(x_0, u, \Delta t) - x_{\ell,m}^k\| \leq (\|x_0 - \bar{x}_\ell\| + |\Delta t - \overline{\Delta t}| k M_f + k \overline{\Delta t} L_u \|u - \bar{u}_m\|) e^{k \overline{\Delta t} L_x},$$

and since ℓ and m are free, we can choose them as $\bar{u}_m := \operatorname{argmin}_{\bar{u} \in \bar{U}} \|u - \bar{u}\|$ and $x_\ell := \operatorname{argmin}_{\bar{x} \in \bar{X}} \|x_0 - \bar{x}\|$. Finally, bounding k by \bar{K} gives (4.9). \square

4.3 Selection of the Shape Parameter

The quality of Shepard approximation strongly depends on the choice of shape parameter σ , both in general for RBF approximation [23] and in the special case of the solution of control problems [28]. As mentioned in the introduction, several techniques exist to tune

the shape parameter in the RBF literature, such as cross validation and maximum likelihood estimation (see e.g. Chapter 14 in [24]), but they are designed to optimize the value of σ in a fixed approximation setting. In our case, on the other hand, we need to construct an approximant at each iteration k within the value iteration (4.2). This makes the existing methods computationally expensive and difficult to adapt to the target of minimizing the error in the iterative method.

For these reasons, we propose here a new method to select the shape parameter based on the minimization of a problem-specific indicator, namely the residual $R(\sigma)$, which is defined as follows. We will denote by V_σ the discrete value function with the choice σ in the Shepard approximation. Assuming that the value iteration with parameter σ has been stopped at iteration k_{final} giving the solution $V_\sigma := V^{k_{\text{final}}}$, we define the residual as

$$R(\sigma) := \|V_\sigma - W_\sigma(V_\sigma)\|_\infty, \quad (4.10)$$

and we choose the shape parameter that minimizes this quantity with respect to $\sigma \in (0, \infty)$.

To get a suitable scale for the value of σ , we parametrize it in terms of the grid X , similarly to what is done in [28] where it is assumed that $\sigma := \theta/h_{\Omega, X}$ for a given $\theta > 0$. Since $h_{\Omega, X}$ is difficult to compute or even to estimate in high dimensional problems, we resort to setting

$$\sigma(\theta) := \theta/q_X, \quad \theta > 0,$$

and we optimize instead the value of $\theta > 0$. Observe that the separation distance q_X is an easily computable quantity that depends only on X , and it is thus actually feasible to use this parametrization even in high dimension.

Choosing an admissible set of parameters $\mathcal{P} := [\theta_{\min}, \theta_{\max}] \subset \mathbb{R}^+$, the parameter is thus chosen by solving the optimization problem

$$\bar{\theta} := \operatorname{argmin}_{\theta \in \mathcal{P}} R(\sigma(\theta)) = \operatorname{argmin}_{\theta \in \mathcal{P}} \|V_{\theta/q_X} - W_{\theta/q_X}(V_{\theta/q_X})\|_\infty. \quad (4.11)$$

Remark 2 This problem can be solved by using a comparison method or e.g. an inexact gradient method. The former means to discretize the set \mathcal{P} as $\{\theta_1, \dots, \theta_{N_p}\} \subset \mathcal{P}$ and to compute all the value functions for all θ_i , $i = 1, \dots, N_p$. The latter considers a projected gradient method where the parameter space \mathcal{P} is continuous and the derivative is computed numerically as

$$R_\theta := \frac{R(\sigma(\theta + \varepsilon)) - R(\sigma(\theta))}{\varepsilon},$$

for some fixed $\varepsilon > 0$. In the numerical tests, we will compare both minimization strategies in the low dimensional case, while we will concentrate on the comparison method in high dimensional one.

4.4 Error Estimates

We adapt the classical convergence theory that is used to prove rates of convergence for the value iteration when linear interpolation is used. In particular, the following argumentation follows the discussion in [22, Section 8.4.1].

The idea is to estimate the time and space discretizations separately. Since the time discretization is independent of the approximation scheme used in the space discretization, we just recall the following result from [22, Section 8.4.1] for a general compact subset Ω . We use the notation $\|f\|_{\infty, \Omega} := \sup_{x \in \Omega} |f(x)|$.

Assumption 2 There exists a (bounded) polyhedron $\Omega \subset \mathbb{R}^d$ such that discrete trajectories $x + \Delta t f(x, u)$ remain in Ω :

$$\forall x \in \Omega, \forall \Delta t \in (0, \frac{1}{\lambda}), \exists u \in U \text{ s.t. } x + \Delta t f(x, u) \in \Omega.$$

Theorem 1 Let us assume that Assumption 1 and Assumption 2 hold true. Let v be the exact value function, and let $v^{\Delta t}$ be the solution of the value iteration (4.2) without space discretization, i.e.,

$$v^{\Delta t}(x) = \min_{u \in U} \left\{ \Delta t g(x, u) + (1 - \Delta t \lambda) v^{\Delta t}(x + \Delta t f(x, u)) \right\}. \tag{4.12}$$

If v is Lipschitz continuous, for each compact subset Ω there exists a constant $C := C(\Omega) > 0$ such that

$$\|v - v^{\Delta t}\|_{\infty, \Omega} \leq C \Delta t^{1/2}. \tag{4.13}$$

Assume additionally that the following hold:

1. f is uniformly bounded, U is convex, $f(x, u)$ is linear in u .
2. $g(\cdot, u)$ is Lipschitz continuous and $g(x, \cdot)$ is convex.
3. There exists an optimal control $u^* \in U$.

Then there exists $C' := C'(\Omega) > 0$ such that

$$\|v - v^{\Delta t}\|_{\infty, \Omega} \leq C' \Delta t. \tag{4.14}$$

It remains now to quantify the error that is committed by introducing a space discretization, i.e., the error associated to the approximation scheme in (4.2). This first requires a bound on the error of Shepard approximation, and we report in the next proposition a result obtained in [28]. In this case, the key idea is to scale the shape parameter of the RBF basis according to the fill distance of the mesh. According to Proposition 1, we can control the fill distance $h_{X, \Omega}$ of the mesh X within the set $\tilde{\Omega}$ obtained as the collection of the different trajectories of the discrete dynamics. In other words, we set

$$\Omega := \Omega(\tilde{X}, \tilde{U}, \tilde{T}) := \left\{ x := x^k(x_0, u, \Delta t) : x_0 \in \tilde{X}, u \in \tilde{U}, \Delta t \in \tilde{T}, k \leq \bar{K} \right\} \tag{4.15}$$

where $\tilde{T} := (0, \frac{1}{\lambda})$ and \tilde{X}, \tilde{U} , are the initial data and the set of controls chosen according to Proposition 1 used to generate the set of trajectories of interest.

For this set, Eq. (4.9) gives

$$\begin{aligned} h_{X, \Omega} &:= \sup_{x \in \Omega} \text{dist}(x, X) \\ &\leq \left(\sup_{\Delta t \in \tilde{T}} |\Delta t - \bar{\Delta t}| \bar{K} M_f + \sup_{x_0 \in \tilde{X}} \min_{\bar{x} \in \tilde{X}} \|\bar{x} - x_0\| + \bar{K} \bar{\Delta t} L_u \sup_{u \in \tilde{U}} \min_{\bar{u} \in \tilde{U}} \|\bar{u} - u\| \right) e^{\bar{K} \bar{\Delta t} L_x}. \end{aligned} \tag{4.16}$$

We can now recall from [28] the error estimate for the Shepard approximation.

Proposition 2 Let $L_v > 0$ be the Lipschitz constant of $v : \Omega \rightarrow \mathbb{R}$. Let S^σ be the Shepard approximation of v on X obtained using a kernel with support contained in $B(0, 1)$, and let $\sigma := C/h_{X, \Omega}$ for a positive constant $C > 0$. Then we have the bound

$$\|v - S^\sigma[v]\|_{\infty, \Omega} \leq CL_v h_{X, \Omega}. \tag{4.17}$$

With these tools, we can finally prove our convergent theorem.

Theorem 2 *Let us assume that Assumption 1 and Assumption 2 hold true. Let Ω be as in (4.15), and assume that \tilde{U} contains the two controls that are optimal for $v^{\Delta t}$ and for V . Then, under the assumptions of Proposition 2 it holds*

$$\|V - v^{\Delta t}\|_{\infty, \Omega} \leq \frac{CL_v}{\lambda} \frac{h_{X, \Omega}}{\Delta t} \tag{4.18}$$

$$\leq \frac{CL_v}{\lambda} \frac{e^{\bar{K}\bar{\Delta t}L_x}}{\Delta t} \left(\sup_{\Delta t \in \bar{T}} |\Delta t - \bar{\Delta t}| \bar{K} M_f + \sup_{x_0 \in \tilde{X}} \min_{\bar{x} \in \tilde{X}} \|\bar{x} - x_0\| + \bar{K} \bar{\Delta t} L_u \sup_{u \in \tilde{U}} \min_{\bar{u} \in \tilde{U}} \|\bar{u} - u\| \right). \tag{4.19}$$

Proof The proof of the first inequality can be found in e.g. [22] and uses Proposition 2 with $v^{\Delta t}$ Lipschitz continuous (see e.g. [9, 10]). The second inequality follows from Proposition 1. □

Finally, we can obtain a complete error estimate by triangular inequality from (4.14) and (4.18) which reads:

$$\|v - V\|_{\infty, \Omega} \leq C' \Delta t + \frac{CL_v}{\lambda} \frac{h_{X, \Omega}}{\Delta t}.$$

4.5 Algorithm

The algorithm to approximate the value function is summarized in Algorithm 1.

Algorithm 1 Value Iteration with shape parameter selection

- 1: INPUT: $\Omega, \Delta t, U, \mathcal{P}$ parameter range, tolerance, RBF and system dynamics $f, ,$
 - 2: initialization
 - 3: Generate Mesh as described in Sect. 4.2
 - 4: **if then**
 - 5: **for** $\theta \in P$ **do**
 - 6: Compute V_θ solving (4.3) with (4.4)
 - 7: $R(\sigma(\theta)) = \|V_{\theta/q_X} - W_{\theta/q_X}(V_{\theta/q_X})\|_\infty$
 - 8: **end for**
 - 9: $\bar{\theta} = \arg \min_{\theta \in P} R(\sigma(\theta))$
 - 10: **else**
 - 11: $R_\theta = 1, \theta = \theta_0, \text{tol}, \varepsilon$
 - 12: **while do**
 - 13: Compute V_θ and $V_{\theta+\varepsilon}$
 - 14: Evaluate $R(V_\theta)$ and $R(V_{\theta+\varepsilon})$ and set $R_\theta = \frac{R(\sigma(\theta + \varepsilon)) - R(\sigma(\theta))}{\varepsilon}$
 - 15: $\theta = \theta - R_\theta$
 - 16: $\theta = \max(\min(\theta_{\max}, \theta), \theta_{\min})$ (projection into \mathcal{P})
 - 17: **end while**
 - 18: $\bar{\theta} = \theta, V_{\bar{\theta}} = V_\theta$
 - 19: **end if**
 - 20: OUTPUT: $\{\bar{\theta}, V_{\bar{\theta}}\}$
-

The computation of the value function via Algorithm 1 allows then to reconstruct the feedback map. It is straightforward using (4.5) where the operator $S^\sigma[V]$ has $\sigma = \bar{\theta}/q_X$ and $V = V_{\bar{\theta}}$. Then, for each discrete interval of size Δt , say $[t_n, t_n + \Delta t)$, the current position x has to be updated. We refer to [22, Section 8.4.6] for more details on the feedback reconstruction.

5 Numerical Experiments

In this section we present three numerical tests to illustrate the proposed algorithm. The first test is a two dimensional minimum time problem with well-known analytical solution. In this test we analyse results using regular and scattered grids. The second and third test deal with an advection equation and a nonlinear heat equation, respectively. We discretize in space both PDEs using finite differences. The dimension of the semi-discrete problem will be 10201 for the advection equation and 961 for the parabolic problem. For each example, we provide examples of feedback and optimal controls reconstructed for different initial conditions that may not belong to the grid. In the parabolic case we present the effectiveness of feedback control under disturbances of the system.

In every experiment we define an admissible interval \mathcal{P} to solve the minimization problem by comparison in Algorithm 1 as follows: we start with a large interval \mathcal{P}_1 and we coarsely discretize it. Then, we run Algorithm 1 and obtain $\hat{\theta}_1$. Later, we choose a set $\mathcal{P}_2 \subset \mathcal{P}_1$ such that $\hat{\theta}_1 \in \mathcal{P}_2$. Using \mathcal{P}_2 and a finer refinement, the Algorithm provides $\hat{\theta}_2$. We iterate this procedure, and finally we set $\mathcal{P} = \mathcal{P}_n$.

In our test we use the Wendland RBF defined in (3.1) The numerical simulations reported in this paper are performed on a laptop with one CPU Intel Core i7–2.2 GHz and 16GB RAM. The codes are written in MATLAB.

Test 1: Eikonal Equation in 2D

We consider a two dimensional minimum time problem in $\Omega = [-1, 1]^2$ with the following dynamics and control space

$$f(x, u) = \begin{pmatrix} \cos(u) \\ \sin(u) \end{pmatrix}, \quad U = [0, 2\pi]. \tag{5.1}$$

The cost functional to be minimized is $\mathcal{J}_x(y, u) = \int_0^{t(x,u)} e^{-s} ds$ with $g = 1, \lambda = 1$ in (2.2) and

$$t(x, u) := \begin{cases} \inf_s \{s \in \mathbb{R}_+ : y_x(s, u) \in \mathcal{T}\} & \text{if } y_x(s, u) \in \mathcal{T} \text{ for some } s \\ +\infty & \text{otherwise,} \end{cases} \tag{5.2}$$

being the time of arrival to the target $\mathcal{T} = (0, 0)$ for each $x \in [-1, 1]^2$.

The analytical solution $V^*(x)$ for this problem is the Kruzkov transform of the distance to the target \mathcal{T} (see e.g. [6]):

$$V^*(x) = 1 - \exp(-v^*(x)), \quad v^*(x) = \|x\|_2, \quad \forall x \in [-1, 1]^2.$$

Observe that v^* is singular at the target point, but it is otherwise smooth.

We tested Algorithm 1 for two different cases. The first one considers an unstructured grid generated by random points, whereas the second case studies an unstructured grid generated by the problem dynamics as mentioned in Sect.4. Due to the randomness of our grid we compute an average dynamics error. In the first case we will average over 10 tests whereas on the second one over 5. For completeness, we also show the results of the proposed method using regular grids with both linear interpolation and Shepard approximant. Finally, in Example 3, we show optimal trajectories discussing the results with all the technique presented.

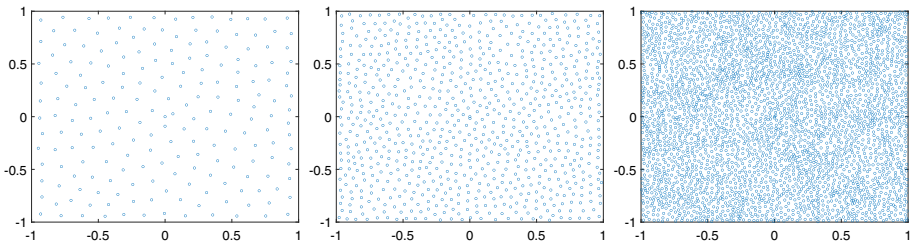


Fig. 2 Example 1. Examples of random generated grids. Left: 200 points and fill distance 0.1618. Center: 800 points and fill distance 0.0846. Right: 3200 points and fill distance 0.0461

The relative error reads:

$$\mathcal{E}(V_\theta) = \frac{\|V_\theta - V^*\|_\infty}{\|V^*\|_\infty} \tag{5.3}$$

where V_θ is the discrete value function obtained with the shape parameter $\sigma = \frac{\theta}{h}$ and V^* is the exact solution. We will denote by θ^* the parameter selected in order to minimize the relative error from (5.3):

$$\theta^* := \arg \min_{\theta \in \mathcal{P}} \mathcal{E}(V_\theta)$$

Clearly, $\mathcal{E}(V_{\theta^*})$ will be a lower bound for $\mathcal{E}(V_\theta)$. In the following three cases U is discretized with 16 equidistant controls.

Example 1 Random Unstructured Grid The first test with Eikonal equation is performed using an unstructured grid generated by random points. In order to obtain a grid which densely covers our numerical domain, a set of 40,000 randomly distributed points in $[-1, 1]^2$ is clustered using the *k-means* algorithm, where k is the number of desired points in the grid. Examples of this type of grid are shown in Fig. 2.

We found $\mathcal{P} = [1, 3]$ a suitable parameter space discretized with 0.1 as step size. In the HJB equation we set $\Delta t = h$. In the left panel of Fig. 3 we see an example of residual $R(\sigma(\theta))$ when the unstructured grid is formed by 3200 nodes. The residual is minimized between 1.5 and 2. Due to the random nature of each grid the optimal value of the parameter θ may vary from case to case. We consider 10 distinct grids obtained as explained in the paragraph above and compute the optimal θ for each grid. For instance, for 3200 points, the average value of θ in these tests is $\bar{\theta} = 1.76$ as can be seen in the fourth column and last row of Table 1. In the middle panel of Fig. 3 we see a plot of $\mathcal{E}(V_\theta)$ for different number of points in the grid; the values θ^* are in the fifth column of Table 1. The right panel of Fig. 3 shows the behavior of $\mathcal{E}(V_{\bar{\theta}})$ and $\mathcal{E}(V_{\theta^*})$ decreasing the fill distance h . The error decays as h does.

Table 1 shows the quality of our results. The first column presents the fill distance h and the correspondent number of points is shown in the second column. The third column presents the average CPU time (in seconds) needed to compute $V_{\bar{\theta}}$. The fourth column presents the values $\bar{\theta}$, outputs of Algorithm 1 using the comparison method in the minimization procedure. The fifth column presents the values of θ^* . The sixth and seventh columns present the values of $\mathcal{E}(V_{\bar{\theta}})$ and $\mathcal{E}(V_{\theta^*})$.

We see the average decay of the fill distance h when increasing the number of nodes. Accordingly, the average CPU time increases. The parameters $\bar{\theta}$ and θ^* assume values close to each other, with $\theta^* > \bar{\theta}$. The errors $\mathcal{E}(V_{\bar{\theta}})$ and $\mathcal{E}(V_{\theta^*})$ reduce according to h . We can also

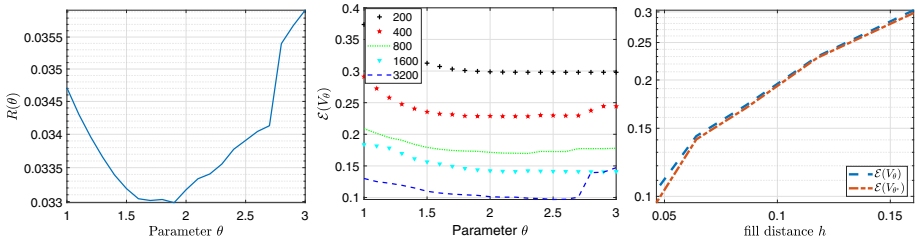


Fig. 3 Example 1. Left: Average residual for 3200 points. Middle: $\mathcal{E}(V_\theta)$. Right: $\mathcal{E}(V_{\bar{\theta}})$ and $\mathcal{E}(V_{\theta^*})$ variation with h

Table 1 Example 1. Numerical Results with random unstructured grid

h	Points	CPU time	$\bar{\theta}$	θ^*	$\mathcal{E}(V_{\bar{\theta}})$	rate	$\mathcal{E}(V_{\theta^*})$	rate
0.1603	200	9.8	1.91	2.16	0.3031		0.2981	
0.1177	400	14.6	1.86	2.06	0.23	0.89	0.2284	0.86
0.0861	800	31.8	1.92	2.21	0.172	0.92	0.1697	0.95
0.0641	1600	115	2.04	2.42	0.1432	0.62	0.1407	0.63
0.0464	3200	504	1.76	2.06	0.1037	0.99	0.0969	1.1

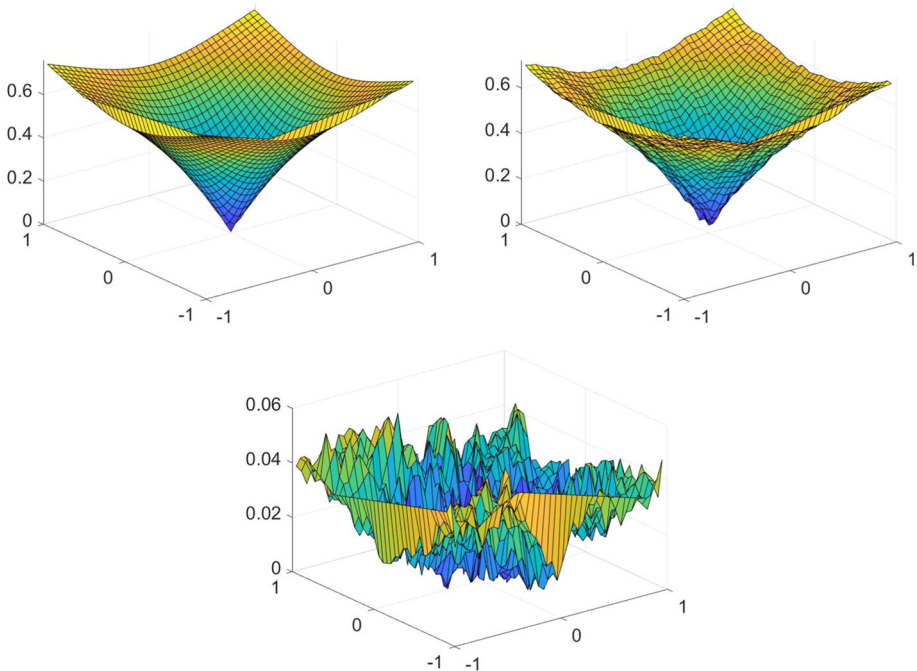


Fig. 4 Example 1. Value Functions generated in a Random Unstructured Grid formed by 3200 points. Left: Exact solution. Center: Solution obtained by VI and Shepard approximation. Right: Absolute error of exact solution and value function obtained by Shepard approximation Value Iteration

Table 2 Example 1. Numerical Results with structured grid and Shepard approximation

h	Points	$\bar{\theta}$	θ^*	$\mathcal{E}(V_{\bar{\theta}})$	rate	$\mathcal{E}(V_{\theta^*})$	rate
0.1	441	0.5	0.5	0.0716	0.64	0.0716	0.26
0.05	1681	0.5	0.5	0.0554	0.37	0.0554	0.37
0.025	6561	0.4	0.4	0.0457	0.28	0.0457	0.28

Table 3 Example 1. Numerical Results with structured grid and standard interpolation

h	Points	$\mathcal{E}(V)$	rate
0.1	441	0.0384	0.3
0.05	1681	0.0274	0.49
0.025	6561	0.0192	0.51

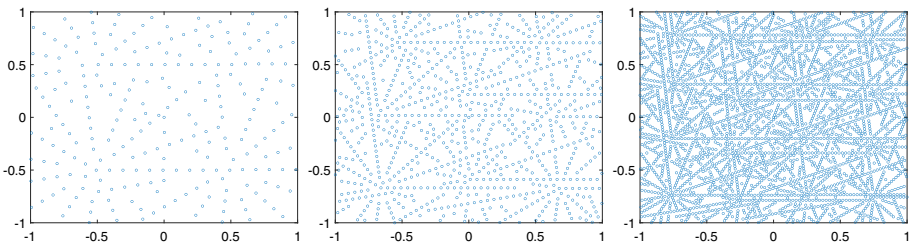


Fig. 5 Example 2. Meshes generated by the dynamics. Left: 246 points, fill distance 0.1436. Middle: 909 points, fill distance 0.0882. Right: 3457 points, fill distance 0.0439. Details on the chosen initial conditions can be found in Table 4

observe the rate of convergence with respect to the parameter h . The behavior of the rate is similar for the choices $\bar{\theta}$ and θ^* .

Figure 4 presents in the left panel the exact solution evaluated on the scattered grid with 3200 points and $h = 0.0464$. The middle picture is the solution obtained by value iteration algorithm with Shepard approximation and the last picture is the absolute error between the two solutions. The error has an erratic behavior always below 10^{-1} .

For the sake of completeness we also show the results with a regular grid and Shepard approximation in Table 2 and with linear interpolation as for e.g. [6, Appendix A] in Table 3. The comparison has been made with the same number of points in the grid and one can see that the order of the error is similar. Clearly, in the proposed approach there are several parameters to tune and also one could choose different kernels. Furthermore, we would like to emphasize that our proposed method aims at working for higher dimensional problems and we suggest to use the standard interpolation routine when dealing with low dimensional problems. We also note that in this case the chosen shape parameter $\bar{\theta}$ coincide with the optimal one θ^* . We do not report the CPU time in Tables 2 and 3 because the choice of \mathcal{P} influences the results and our focus is to compare the accurateness of the results.

Example 2 Grid driven by the dynamics In this example we test our novel grid proposed in Sect. 4. We set $\Delta t = h$ in the HJB equation. To generate the trajectories which will be our grid points, we set $(\bar{\Delta}t, \bar{L}, \bar{M}) = \{(0.1, 4, 16), (0.05, 8, 16), (0.025, 16, 16)\}$ in (4.7). Figure 5 shows some examples of meshes generated in this case, with randomly selected initial conditions. These meshes follow the pattern of problem dynamics.

Table 4 Example 1. Initial conditions \bar{X} , number of points N , and fill distance h , for the three examples of Fig. 5

N	h	\bar{X}
246	0.1436	$\{(0.497, 0.499), (-0.495, -0.497), (0.502, -0.502), (-0.504, 0.499)\}$
909	0.0882	$\{(-0.022, 0.542), (0.001, -0.532), (0.666, -0.672), (-0.667, 0.668), \dots$ $(0.591, 0.0142), (0.653, 0.689), (-0.594, -0.017), (-0.664, -0.683)\}$
3457	0.0439	$\{(-0.794, 0.244), (0.754, 0.764), (-0.247, 0.741), (-0.181, -0.271), \dots$ $(-0.757, -0.750), (-0.743, 0.747), (0.704, 0.294), (0.253, 0.746), \dots$ $(0.319, -0.225), (-0.257, -0.760), (0.253, -0.739), (0.148, 0.249), \dots$ $(-0.717, -0.255), (-0.343, 0.215), (0.778, -0.197), (0.755, -0.736)\}$

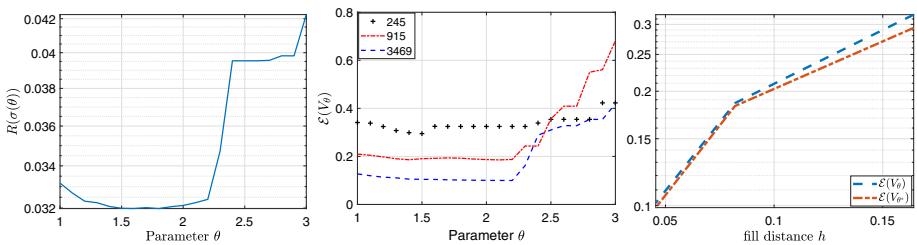


Fig. 6 Example 2. Left: Average residual to case with 3469 points. Middle: $\mathcal{E}(V_\theta)$. Right: $\mathcal{E}(V_{\bar{\theta}})$ and $\mathcal{E}(V_{\theta^*})$ variation with h

Table 5 Example 2. Numerical results with a grid driven by the dynamics

h	Points	CPU time	$\bar{\theta}$	θ^*	$\mathcal{E}(V_{\bar{\theta}})$	Rate	$\mathcal{E}(V_{\theta^*})$	Rate
0.1642	245	8.5	1.58	1.82	0.3182		0.2949	
0.0820	915	55.6	1.66	1.76	0.1861	1.29	0.1855	1.49
0.0455	3469	654	1.7	1.82	0.1016	0.97	0.0997	0.94

We set, again, $\mathcal{P} = [1, 3]$. The behavior of $R(\sigma(\theta))$ is shown in Fig. 6 when the grid has 3469 points on average. The minimum value is achieved for $\bar{\theta} = 1.7$. The middle panel of Fig. 6 shows a plot of $\mathcal{E}(V_\theta)$ for a different number of points. The right picture shows the error behavior in $\mathcal{E}(V_{\bar{\theta}})$ and $\mathcal{E}(V_{\theta^*})$ with the reduction of h . It decreases according to Theorem 2. We stress that all of these quantities are computed averaging 5 simulations.

Table 5 summarizes the results of Example 2 as discussed in Example 1. All the considerations are very similar to the previous example but now we have a different grid which will help us to deal with higher dimensional problems as it will be presented in the next sections. We stress that the values of the error indicator in the sixth and eighth column of Table 5 are very close to each other. Once again, this is very interesting since we are using an a-posteriori criteria for the computation of the shape parameter. We can also observe that the rate of convergence with respect to the choice of $\bar{\theta}$ and θ^* is similar.

Finally, Table 6 presents the results of Algorithm 1 using a gradient descent method with $\varepsilon = 10^{-6}$ in step 11 of Algorithm 1. If we compare the results with Table 5 we can see that this method is computationally slower and the accuracy has the same of order of the comparison method. Thus, we will only show the performance of our method where the minimization is

Table 6 Example 2. Results using gradient method

h	Points	CPU time	$\bar{\theta}$	$\mathcal{E}(V_{\bar{\theta}})$
0.1364	248	9.7	1.62	0.278
0.0865	924	152	1.72	0.1859

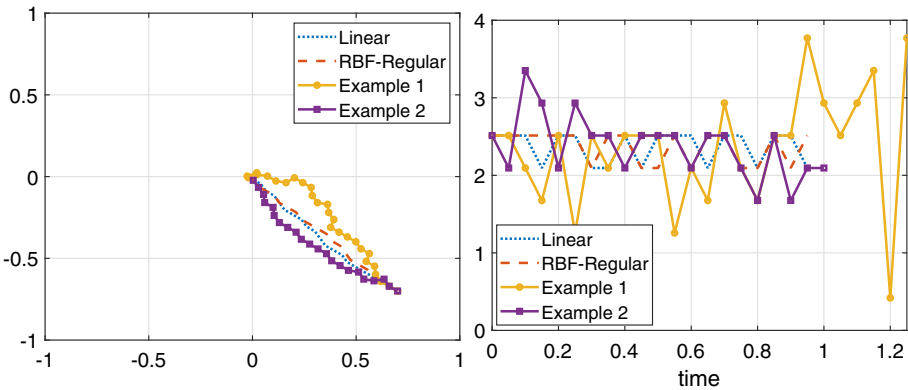


Fig. 7 Example 3. Optimal trajectories (left) and optimal controls (right) for $x = (0.7, -0.7)$

computed by comparison. We do not provide results with smaller h in Table 6 because it is clear that it will be way slower than the comparison method.

Example 3 On the feedback reconstruction.

The approximated value functions computed by means of Algorithm 1 with different grids allows us to obtain the optimal trajectories and optimal controls for any initial conditions. In Fig. 7, we present an example of optimal controls and trajectories computed for $x = (0.7, -0.7)$ using value functions obtained in Examples 1 and 2. For completeness, we also show the results considering the value function obtained by traditional value iteration algorithm using linear interpolation and Shepard method on a regular grid. The latter comes from [28].

All trajectories reach the target \mathcal{T} but with different costs. The value of the cost functional, for a given initial condition, is equal when dealing with a structured grid with linear interpolation and Shepard approximation. The value of cost functional with value function from Example 2 is always smaller or equal than the value of cost functional from Example 1, for both initial conditions.

In Table 7 we provide the evaluation of the cost functional for different initial conditions and different methods whereas in Table 8 we provide the arrival time at the target. It is interesting to see that linear interpolation and Shepard approximation coincide on a equidistributed grid and that the use of Shepard with a grid driven by the dynamics lead to lower cost functional values with respect to the random mesh.

Table 7 Example 3. Evaluation of the cost functional for different methods and initial conditions x

x	Linear	RBF-Regular	Example 1	Example 2
$(-0.7, -0.7)$	0.6664	0.6664	0.7006	0.7006
$(0.7, 0.7)$	0.6664	0.6664	0.7164	0.6839
$(-0.7, 0.7)$	0.6664	0.6664	0.8076	0.6839
$(0.7, -0.7)$	0.6664	0.6664	0.7594	0.6839

Table 8 Example 3. Arrival time at the target (in seconds) for different methods and initial conditions x

x	Linear	RBF-Regular	Example 1	Example 2
$(-0.7, -0.7)$	1	1	1.1	1.1
$(0.7, 0.7)$	1	1	1.15	1.05
$(-0.7, 0.7)$	1	1	1.5	1.05
$(0.7, -0.7)$	1	1	1.3	1.05

Test 2: Bilinear Advection Equation

The second test deals with the control of a two-dimensional advection equation with constant velocity $\zeta \in \mathbb{R}$:

$$\begin{cases} \tilde{y}_t(\xi, t) + \zeta \nabla_{\xi} \tilde{y}(\xi, t) = u(t) \tilde{y}(\xi, t) & (\xi, t) \in \Xi \times [0, T] \\ \tilde{y}(\xi, t) = 0 & \xi \in \partial \Xi \times [0, T] \\ \tilde{y}(\xi, 0) = \tilde{y}_0(\xi) & \xi \in \Xi. \end{cases} \tag{5.4}$$

where $\Xi = [0, 5]^2$, $\zeta = 1$ and $T = 2.5$ is chosen large enough to simulate the infinite horizon problem. Equation (5.4) can be written in form (2.1) using finite differences spatial discretization (see e.g. [32]) which leads to a system of ODEs:

$$\begin{cases} \dot{y}(t) = Ay(t) + u(t)y(t) & t \in (0, T], \\ y(0) = y_0 \in \mathbb{R}^d \end{cases} \tag{5.5}$$

where $A \in \mathbb{R}^{d \times d}$ is the discretization of the gradient term, $y(t) \in \mathbb{R}^d$ corresponds to the approximation of $\tilde{y}(\xi, t)$ at the grid points, $(y_0)_i = \tilde{y}_0(\xi_i)$, $i = 1, \dots, d$ with $\xi_i \in \Xi$ being a node of the discretization of Ξ and control $u(t) \in U$. Our goal is to steer the solution $y(t)$ of (5.5) as close as possible to the value 0, minimizing the following cost functional:

$$\mathcal{J}_x(y, u) \equiv \int_0^T (\|y(s)\|_2^2 + \gamma |u(s)|^2) e^{-\lambda s} ds \tag{5.6}$$

where $\gamma = 10^{-5}$ and $y(t)$ solves (5.5).

In this test we select initial conditions from a class of parametrized functions:

$$\mathcal{C} := \{ \kappa \sin(\pi x_1) \sin(\pi x_2) \chi_{[0,1]^2}; \kappa \in (0, 1] \}. \tag{5.7}$$

To generate the grid driven by the dynamics we have chosen $\kappa = \{0.5, 1\}$ in (5.7), 11 controls equidistributed in $U = [-2, 0]$ and $\bar{\Delta}t = 0.1$. Thus, in (4.7), we set: $\bar{\Delta}t = 0.1$; $\bar{M} = 11$; $\bar{L} = 2$. Equation (5.5) is then solved for each initial condition and each control with Ξ discretized with $d = 10201$ points, and the time interval $[0, 2.5]$. step size $\Delta t = 0.05$. After computing

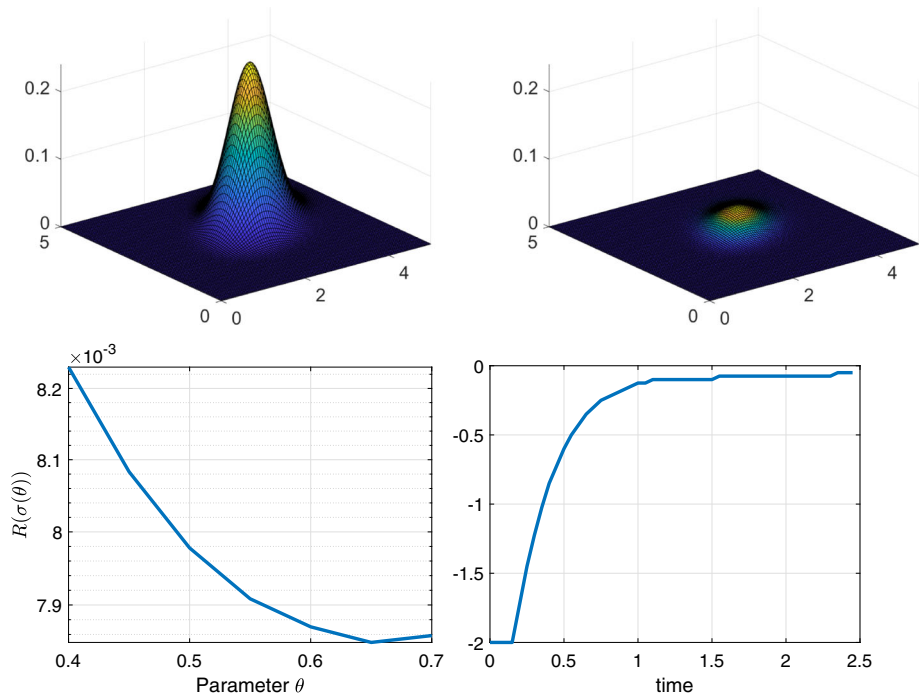


Fig. 8 Test 2. Initial condition $y(x, 0) = 0.75\sin(\pi x_1)\sin(\pi x_2)\chi_{[0,1]^2}$. Top: uncontrolled solution (left) and controlled solution (right). Bottom: residual (left) and optimal control (right)

the grid generated by the dynamics, we run Algorithm 1 with $\mathcal{P} = [0.4, 0.7]$ discretized with step size 0.05, fixing $\Delta t = 0.05$ to discretize (5.5) by an implicit Euler method and 21 equidistributed controls. The residual $R(\sigma(\theta))$ reaches its minimum with $\bar{\theta} = 0.65$ as shown in the bottom-left panel of Fig. 8. The CPU time to run our algorithm is 583.6 s.

To obtain the feedback control and optimal trajectories we have enlarged the set of discrete controls U with 81 points (in the value function we used 21 controls). Thus, we have studied the control problem for different initial conditions selected from the set (5.7) using the value function already stored. In Fig. 8 we can compare in the top panels the uncontrolled solution, i.e. $u(t) = 0$, with controlled solution for $y(x, 0) = 0.75 \sin(\pi x_1) \sin(\pi x_2)\chi_{[0,1]^2}$. The respective optimal control is shown in the bottom-right panel of Fig. 8. Note that this initial condition does not belong to the grid.

We have also studied the following initial conditions: $\kappa = \{0.5, 1\}$ in (5.7). The behavior of the solution is similar to Fig. 8. We show a plot of the cost functionals in Fig. 9, and we see that the controlled solution has always a lower cost functional than the uncontrolled solutions. We are able to reach the desired configuration with the three initial conditions considered ($\kappa = \{0.5, 0.75, 1\}$ in (5.7)).

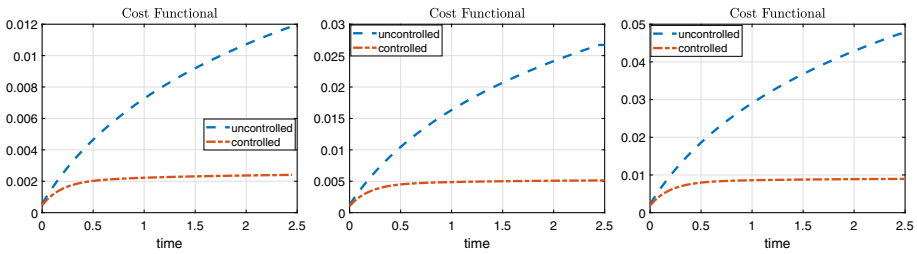


Fig. 9 Test 2. Cost functional. Left: $y(x, 0) = 0.5\sin(\pi x_1)\sin(\pi x_2)\chi_{[0,1]^2}$. Center: $0.75y(x, 0) = \sin(\pi x_1)\sin(\pi x_2)\chi_{[0,1]^2}$. Right: $y(x, 0) = \sin(\pi x_1)\sin(\pi x_2)\chi_{[0,1]^2}$

Test 3: Nonlinear Heat Equation

This test deals with the control of a two-dimensional parabolic equation with polynomial nonlinearities:

$$\begin{cases} \tilde{y}_t(\xi, t) = \alpha \Delta \tilde{y}(\xi, t) + \beta(\tilde{y}^2(\xi, t) - \tilde{y}^3(\xi, t)) + u(t)\tilde{y}_0(\xi) & (\xi, t) \in \Xi \times [0, T) \\ \partial_n \tilde{y}(\xi, t) = 0 & \xi \in \partial \Xi \times [0, T) \\ \tilde{y}_0(\xi) = \tilde{y}(\xi, 0) & \xi \in \Xi \end{cases} \quad (5.8)$$

with $\Xi = [0, 1] \times [0, 1]$, $\alpha = \frac{1}{100}$, $\beta = 6$, $T = 5$. Finite differences in space for (5.8) leads to

$$\begin{cases} \dot{y}(t) = Ay(t) + Bu(t) + f(y(t)) & t \in (0, T) \\ y(0) = y_0 \in \mathbb{R}^d \end{cases} \quad (5.9)$$

where $A \in \mathbb{R}^{d \times d}$ is the discretization of the laplacian, $B \in \mathbb{R}^d$ where $B_i = \tilde{y}_0(\xi_i)$ for $i = 1, \dots, d$ and ξ_i a node of the discretization of Ξ . Here the nonlinear term $f : \mathbb{R}^d \rightarrow \mathbb{R}^d$ is $f(y(t)) = y(t)^2 - y(t)^3$.

We want to minimize again (5.6) as in the previous test and consider the class (5.7) of initial conditions. Here, we build an unstructured mesh using as initial condition with $\kappa = \{0.5, 1\}$ in (5.7). In (4.7), we set $\Delta t = 0.1$, $\bar{M} = 41$, $\bar{L} = 2$. The state space $\Xi = [0, 1]^2$ was discretized in 31^2 points which is the dimension of the discretized problem (5.9). The control space $U = [-2, 0]$ is discretized with 41 points. The time domain was discretized in 51 points. We set $\gamma = 10^{-2}$ in (5.6) and run Algorithm 1 using $\mathcal{P} = [2, 2.4]$ with step size of 0.025 and $\Delta t = 0.075$. The parameter that minimizes $R(\sigma(\theta))$ is $\bar{\theta} = 2.225$ as shown in Fig. 10. higher values. The time needed to approximate the value function is approximately 40 minutes.

We present the controlled solutions for different initial conditions taken from \mathcal{C} in (5.7). First, we consider the initial condition $y(x, 0) = 0.75 \sin(\pi x_1) \sin(\pi x_2)$ and the results are shown in Fig. 11. As one can see in the left panel the solution reach the unstable equilibrium $y(t) = 1$, whereas the controlled solution goes to 0 as desired. The optimal control, computed as discussed in Sect. 4.5 is then shown in the right panel of Fig. 11. Note that the initial condition does not belong to the grid where we computed the value function.

Figure 12 presents the evaluation of the cost functional for the initial conditions considered. As expected, the cost of controlled solutions is always smaller than costs of uncontrolled solutions.

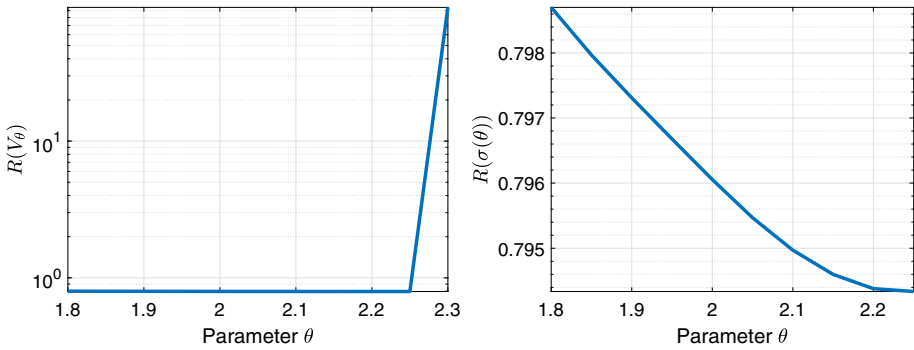


Fig. 10 Test 3. Residual

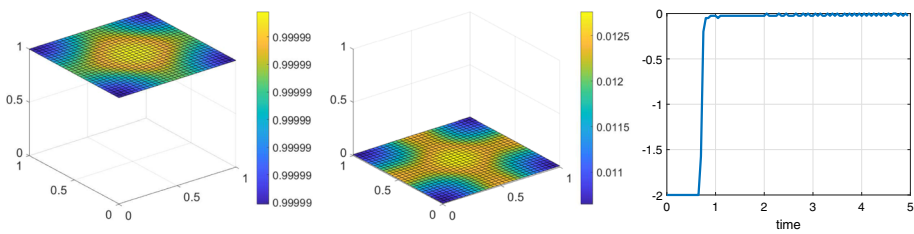


Fig. 11 Test 3. Initial condition $y(x, 0) = 0.75 \sin(\pi x_1) \sin(\pi x_2)$. Left: uncontrolled solution at time $t = 5$. Middle: controlled solution at time $t = 5$. Right: optimal control

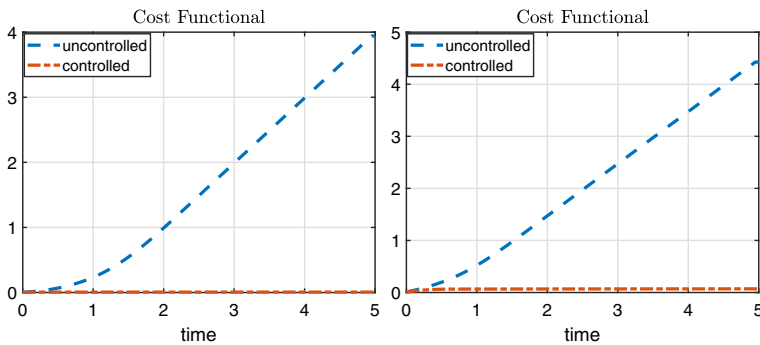


Fig. 12 Test 3. Cost functional. Left: $y(x, 0) = 0.5\sin(\pi x_1)\sin(\pi x_2)$. Center: $0.75y(x, 0) = \sin(\pi x_1)\sin(\pi x_2)$. Right: $y(x, 0) = \sin(\pi x_1)\sin(\pi x_2)$

We now check the robustness of the method adding a noise term at each time instance. We keep using the same value function stored before and we computed the optimal trajectory for an initial condition with a small perturbation. Here we consider $y(x, 0) = 0.75 \sin(\pi x_1) \sin(\pi x_2) + \mathcal{N}(0, 0.025)$ where $\mathcal{N}(0, 0.025)$ is a normally distributed random variable with mean zero and standard deviation 0.025. With these parameters we have a probability of 95, 45% of selecting a number in the range $[-0.05, 0.05]$ at each iteration. At each time iteration a new independent perturbation $\mathcal{N}(0, 0.025)$ has been added to the trajectory. Left picture of Fig. 13 presents the uncontrolled trajectory and the solution converges (somehow) to $y(x) = 1$ with a perturbation. The middle panel shows the controlled solution

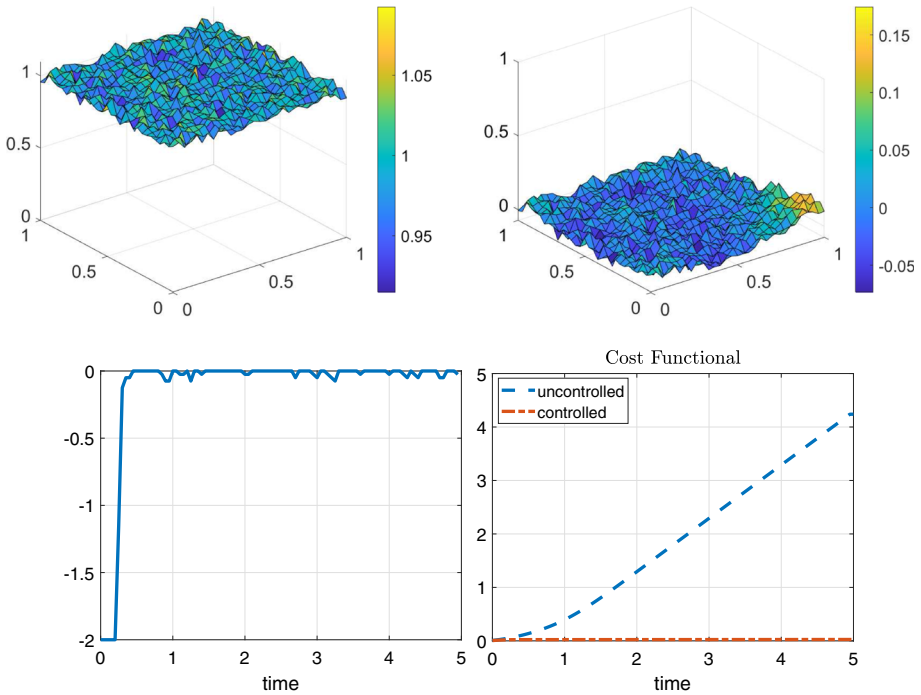


Fig. 13 Test 3. Initial condition $y(x, 0) = 0.75\sin(\pi x_1)\sin(\pi x_2) + \mathcal{N}(0, 0.025)$. Left: uncontrolled solution. Middle: controlled solution. Right: optimal control. Running Cost with initial condition $y(x, 0) = 0.75\sin(\pi x_1)\sin(\pi x_2) + \mathcal{N}(0, 0.025)$

and how it is close to $y(x) = 0$, also with a perturbation. The left panel in the bottom line of Fig. 13 presents the optimal control. A comparison of the cost functional for the perturbed problem is shown in the bottom right panel of Fig. 13.

Finally, to further show the effectiveness of our method we consider a non-smooth initial condition that does not belong to (5.7):

$$y(x, 0) = \max\{-2|x - 0.5| + 1\}(2|y - 0.5| + 1) + 2, 0\}$$

as shown in the top left panel of Fig. 14. Here we consider a time interval $T = [0, 8]$ discretized in 161 points.

Figure 14 shows the uncontrolled trajectory, which converges to $y(x) = 1$ and the controlled trajectory, which converges to the unstable equilibrium $y(x) = 0$ as desired. Figure 15 also presents the optimal control and the evaluation of the cost functional.

6 Conclusions and Future Works

We have proposed a novel method to approximate stationary HJB equations using RBF and Shepard approximation. The RBF usually presents a parameter which is here selected by means of a-posteriori criteria. We have also shown a new way to generate the grid which helps to deal with high dimensional problems localizing the problem along trajectories of interest. This method has the advantage to be able to reconstruct the feedback for (a class of)

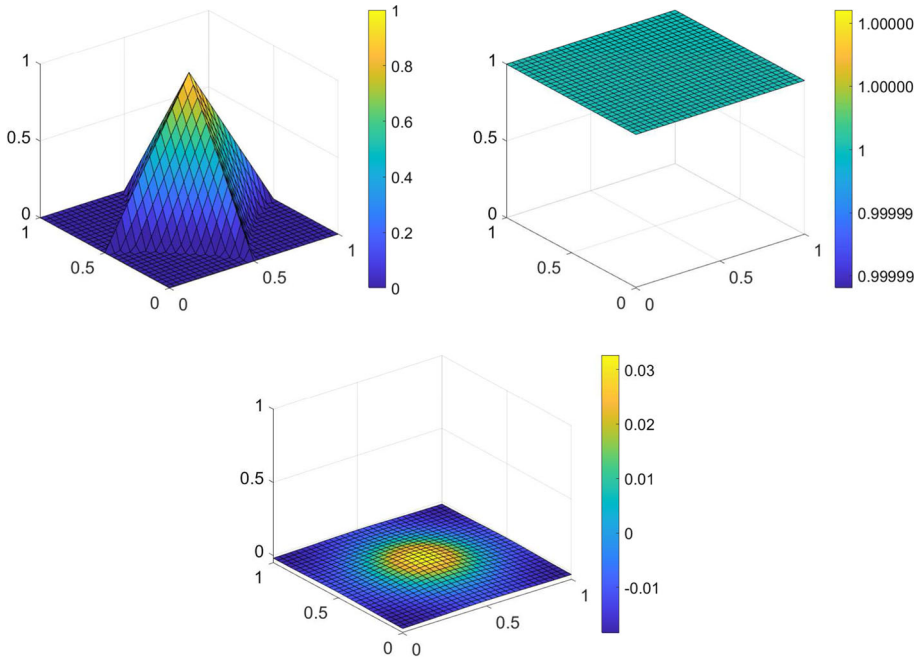


Fig. 14 Test 3. Left: Initial condition $y(x, 0) = \max\{-(2|x - 0.5| + 1)(2|y - 0.5| + 1) + 2, 0\}$. Middle: uncontrolled solution. Right: controlled solution

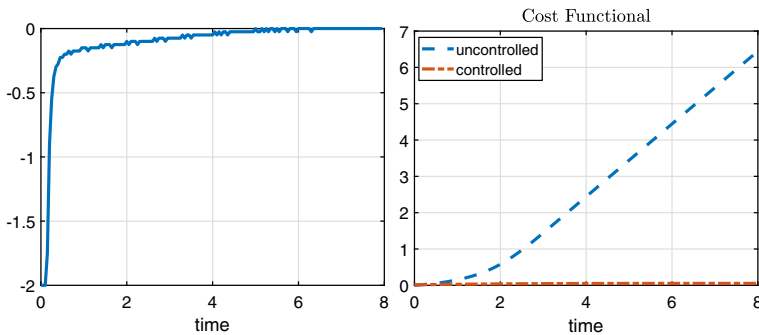


Fig. 15 Test 3. Left: optimal control and (right) running Cost with initial condition $y(x, 0) = \max\{-(2|x - 0.5| + 1)(2|y - 0.5| + 1) + 2, 0\}$

initial conditions without the need of update the mesh or recompute the HJB approximation as usually happens for the control of PDE with a DP approach. We have also provided an error estimate for the value function and proved, by numerical evidence, the effectiveness of our method. The method could be extended to the semi-Lagrangian schemes where the approximation is needed to reconstruct the characteristic of the problem. Furthermore, it

will be our interest to couple this method with Model Order Reduction to deal with more sophisticated PDE example, and possibly industrial applications.

Funding AA was supported by the CNPq research grant 3008414/2019-1 and by a research grant from PUC-Rio. HO was supported by the Coordenação de Aperfeiçoamento de Pessoal de Nível Superior - Brasil (CAPES).

Data Availability Enquiries about code availability should be directed to the authors. No data has been used in this paper.

Declarations

Conflict of interest No conflict of interest.

References

1. Alla, A., D'Elia, M., Glusa, C., Oliveria, A.H.: Control of fractional diffusion problems via dynamic programming equations. *J. Peridyn. Nonlocal. Model* (2023). <https://doi.org/10.1007/s42102-023-00101-z>
2. Alla, A., Falcone, M., Kalise, D.: An efficient policy iteration algorithm for dynamic programming equations. *SIAM J. Sci. Comput.* **3**(7), 181–200 (2015)
3. Alla, A., Falcone, M., Saluzzi, L.: An efficient DP algorithm on a tree-structure for finite horizon optimal control problems. *SIAM J. Sci. Comput.* **41**, A2384–A2406 (2019)
4. Alla, A., Falcone, M., Volkwein, S.: Error analysis for POD approximations of infinite horizon problems via the dynamic programming approach. *SIAM J. Control Optim.* **55**, 3091–3115 (2017)
5. Alla, A., Saluzzi, L.: A HJB-POD approach for the control of nonlinear PDEs on a tree structure. *Appl. Numer. Math.* **155**, 192–207 (2020)
6. Bardi, M., Capuzzo-Dolcetta, I.: *Optimal Control and Viscosity Solutions of Hamilton–Jacobi–Bellman Equations*. Birkhäuser, Basel (1997)
7. Benner, P., Gugercin, S., Willcox, K.: A survey of projection-based model reduction methods for parametric dynamical systems. *SIAM Rev.* **57**, 483–531 (2015)
8. Bokanowski, O., Garcke, J., Griebel, M., Klompaker, I.: An adaptive sparse grid semi-Lagrangian scheme for first order Hamilton–Jacobi Bellman equations. *J. Sci. Comput.* **55**, 575–605 (2013)
9. Capuzzo Dolcetta, I., Ishii, H.: Approximate solutions of the Bellman equation of deterministic control theory. *Appl. Math. Optim.* **11**, 161–181 (1984)
10. Capuzzo Dolcetta, I.: On a discrete approximation of the Hamilton–Jacobi equation of dynamic programming. *Appl. Math. Optim.* **10**, 367–377 (1983)
11. Carlini, E., Falcone, M., Ferretti, R.: An efficient algorithm for Hamilton–Jacobi equations in high dimension. *Comput. Vis. Sci.* **7**, 15–29 (2004)
12. Carlini, E., Ferretti, R.: A semi-Lagrangian scheme with radial basis approximation for surface reconstruction. *Comput. Vis. Sci.* **18**, 103–112 (2017)
13. Chen, W., Fu, Z.-J., Chen, C.-S.: Recent advances in radial basis function collocation methods. *Briefs Appl. Sci. Technol.* (2014). <https://doi.org/10.1007/978-3-642-39572-7>
14. Chilan, C.M., Conway, B.A.: Optimal nonlinear control using Hamilton–Jacobi–Bellman viscosity solutions on unstructured grids. *J. Guid. Control Dyn.* **43**, 30–38 (2020)
15. Darbon, J., Osher, S.J.: Splitting enables overcoming the curse of dimensionality. In: Glowinski, R., Osher, S., Yin, W. (eds.) *Splitting Methods in Communication, Imaging, Science, and Engineering*. Scientific Computation. Springer, Cham (2016)
16. Darbon, J., Osher, S.: Algorithms for overcoming the curse of dimensionality for certain Hamilton–Jacobi equations arising in control theory and elsewhere. *Res. Math. Sci.* **3**, 19–26 (2016)
17. Dolgov, S., Kalise, D., Kunisch, K.: Tensor decomposition for high-dimensional Hamilton–Jacobi–Bellman equations, submitted, 2019. <https://arxiv.org/pdf/1908.01533.pdf>
18. Dolgov, S., Kalise, D., Saluzzi, L.: Data-driven tensor train gradient cross approximation for Hamilton–Jacobi–Bellman equations, submitted, 2022. [arxiv:2205.05109](https://arxiv.org/abs/2205.05109)
19. Ehring, T., Haasdonk, B.: Feedback control for a coupled soft tissue system by kernel surrogates. In: *Proceedings of COUPLED 2021* (2021)

20. Ehring, T., Haasdonk, B.: Greedy sampling and approximation for realizing feedback control for high dimensional nonlinear systems. *IFAC-PapersOnLine* **55**, 325–330 (2022)
21. Falcone, M., Ferretti, M.R.: Discrete time high-order schemes for viscosity solutions of Hamilton–Jacobi–Bellman equations. *Numer. Math.* **67**, 315–344 (1994)
22. Falcone, M., Ferretti, R.: Semi-Lagrangian Approximation Schemes for Linear and Hamilton-Jacobi equations. *SIAM* (2013). <https://doi.org/10.1137/1.9781611973051>
23. Fasshauer, G.F.: Meshfree approximation methods with MATLAB (2007)
24. Fasshauer, G.F., McCourt, M.: Kernel-based approximation methods using MATLAB (2015)
25. Ferretti, G., Ferretti, R., Junge, O., Schreiber, A.: An adaptive multilevel radial basis function scheme for the HJB equation. *IFAC-PapersOnLine* **50**, 1643–1648 (2017)
26. Fornberg, B., Flyer, N.: Solving PDEs with radial basis functions. *Acta Numer.* **24**, 215–258 (2015)
27. Garcke, J., Kröner, A.: Suboptimal feedback control of PDEs by solving HJB equations on adaptive sparse grids. *J. Sci. Comput.* **70**, 1–28 (2017)
28. Junge, O., Schreiber, A.: Dynamic programming using radial basis functions. *Discrete Contin. Dyn. Syst.-Ser. A* **35**, 4439–4453 (2015)
29. Grüne, L.: An adaptive grid scheme for the discrete Hamilton–Jacobi–Bellman equation. *Numerische Mathematik* **75**, 319–337 (1997)
30. Kalise, D., Kunisch, K.: Polynomial approximation of high-dimensional Hamilton–Jacobi–Bellman equations and applications to feedback control of semilinear parabolic PDEs. *SIAM J. Sci. Comput.* **40**, A629–A652 (2018)
31. Kunisch, K., Volkwein, S., Xie, L.: HJB-POD based feedback design for the optimal control of evolution problems. *SIAM J. Appl. Dyn. Syst.* **4**, 701–722 (2004)
32. Leveque, R.J.: Finite difference methods for ordinary and partial differential equations: steady-state and time-dependent problems. *SIAM* (2007). <https://doi.org/10.1137/1.9780898717839>
33. McEneaney, W.M.: Convergence rate for a curse-of-dimensionality-free method for Hamilton–Jacobi–Bellman PDEs represented as maxima of quadratic forms. *SIAM J. Control Optim.* **48**, 2651–2685 (2009)
34. McEneaney, W.M.: A curse-of-dimensionality-free numerical method for solution of certain HJB PDEs. *SIAM J. Control Optim.* **46**, 1239–1276 (2007)
35. Schmidt, A., Haasdonk, B.: Data-driven surrogates of value functions and applications to feedback control for dynamical systems. *IFAC-PapersOnLine* **51**, 307–312 (2018)
36. Wendland, H.: Piecewise polynomial, positive definite and compactly supported radial functions of minimal degree. *Adv. Comput. Math.* **4**, 389–396 (1995)
37. Wendland, H.: Scattered data approximation. Cambridge University Press, Cambridge (2004)

Publisher’s Note Springer Nature remains neutral with regard to jurisdictional claims in published maps and institutional affiliations.

Springer Nature or its licensor (e.g. a society or other partner) holds exclusive rights to this article under a publishing agreement with the author(s) or other rightsholder(s); author self-archiving of the accepted manuscript version of this article is solely governed by the terms of such publishing agreement and applicable law.